Cellulose
DOI 10.1007/s10570-014-0517-7

ORIGINAL PAPER

Isolation of cellulose nanocrystals from onion skin and their utilization for the preparation of agar-based bio-nanocomposites films

Jong-Whan Rhim · Jeevan Prasad Reddy · Xiaogang Luo

Received: 10 April 2014 / Accepted: 25 November 2014

Abstract Cellulose nanocrystals (CNC) were isolated from onion skin using different concentrations of acid (45, 55, and 65 % H_2SO_4) and agar/CNC composite films were prepared to test their performance properties. The major component of onion skin was α-Cellulose (41.1 %). The yield, crystallinity index (CI), crystallite size, and thermal stability of the CNC varied depending on the acid concentration. The CNC isolated with 45 % of H_2SO_4 (CNC45) had the highest yield (48.6 %), CI (0.26), crystallite size (2.49 nm), and thermal stability among the tested CNCs. Performance test results of agar/CNCs composite films also indicated that the CNC45 reinforced composite film had the highest tensile strength (TS: 50 MPa) and Young's modulus (YM: 1.98 GPa) with the lowest water vapor permeability (WVP: 1.78×10^{-9} g m/m^2 s Pa). The properties of agar/CNC45 composite films were also greatly influenced by the content of nanofiller. The composite film exhibited the maximum strength and water vapor barrier properties with 3 wt% inclusion of CNC45. The present study revealed that the onion skin is an interesting new source of cellulose material for the preparation of bio-nanocomposite materials.

Keywords Onion skin · Microcrystalline fiber · Cellulose nanofiber · Agar · Bio-nanocomposite

J.-W. Rhim (✉) · J. P. Reddy
Department of Food Engineering and Bionanocomposite Research Institute, Mokpo National University, 61 Dorimri, Chungkyemyon, Muangun, Jeonnam 534-729, Republic of Korea
e-mail: jwrhim@mokpo.ac.kr

X. Luo
School of Chemical Engineering and Pharmacy, Wuhan Institute of Technology, 693 Xiongchu Avenue, Wuhan 430073, Hubei, People's Republic of China

Introduction

Recently, there has been increasing interest in lignocellulosic materials for the production of novel biodegradable or biocompatible composite materials for the biomedical, food packaging, and other industrial applications due to their ecological and renewable nature (Siro and Plackett 2010; Khan et al. 2014). Lignocellulosic materials are composed of cellulose, hemi-cellulose, lignin, and a smaller amount of extractives (Komolwanich et al. 2014). Major sources of lignocellulosic materials include woods, plant and vegetable stalks, straw, leaves, roots, husk, nut, and seed shells. In addition, large amounts of lignocellulosic waste or by-products are generated annually through forestry and agricultural practices, paper pulp industries, timber industries, and many other agro-industries (Limayema and Ricke 2012). One of the value-added methods for the use of these lignocellulosic biomass is the production of cellulose nanofibers or whiskers to develop green nanocomposites (Hubbe

Published online: 29 November 2014

et al. 2008). Generally, cellulose nanofibers or nanocelluloses are produced by the disintegration of plant celluloses using shear forces or controlled hydrolysis of wood pulp (Khan et al. 2014). Various physical (high pressure homogenization) (Herrick et al. 1983), chemical (acid hydrolysis) (Beck-Candanedo et al. 2005; Reddy and Rhim 2014), and biological (enzymatic hydrolysis) (Henriksson et al. 2007) methods have been established for the isolation of nanocellulose. Among them, acid hydrolysis is the most widely used method to prepare cellulose nanowhiskers (Bondeson et al. 2006). Acid hydrolysis is a surface phenomenon attacking amorphous part of the cellulose and obtaining the highly ordered crystalline structure. The structural properties of nanocellulose obtained by acid hydrolysis depend on many factors such as cellulose source, acid type and concentration, acid to cellulosic fiber ratio, and hydrolysis time and temperature (Bondeson et al. 2006; Ludueina et al. 2011; Ioelovich 2012a).

Various lignocellulosic resources generated from agricultural or food processing industries have been used for the isolation of cellulose nanofibers or whiskers to test their potential use for the preparation of biocomposite (Yu et al. 2006). Alemdar and Sain. (2008) extracted cellulose nanofibers from the agricultural residues such as wheat straw and soy hulls by using chemical and mechanical methods to test their potential use as reinforcement fibers in biocomposite formation. Oksman et al. (2011) extracted cellulose nanowhiskers from industrial bio-residues as a source of raw material. Santos et al. (2013) isolated cellulose nanowhiskers from an annually renewable agricultural residue pineapple leaf.

As one of underutilized lignocellulose sources, onion skins are interesting since they are abundantly produced in the food processing industry as a waste or by-product. Onion skins are outer layers of onion bulb which are peeled off and discarded as waste in the food processing industry. Onion (*Allium cepa* L.) is a commonly used condiment vegetable which is the sixth most widely used vegetable in the world. Every year, more than half million tons of onion skins are thrown away as waste in the European Union (Benítez et al. 2011). Although onion skins are rich in functional ingredients including fibers and functional phenolic compounds such as quercetin and other flavonoids (Benítez et al. 2011), only a limited number of efforts have been attempted to exploit the material for the industrial use. Onion skins have been used for dyeing fabrics, cotton, and paper (Akaranta and Efanga 1997; Padma and Rakhi 2009). However, to the best of our knowledge, there has no reported works in the literature on the extraction and characterization of cellulose nanocrystals from onion skins for the utilization as a reinforcing material for the preparation of bionanocomposites.

Considerable research efforts have been focused on the development of completely biodegradable composite materials by blending cellulose nanofibers with bioplastics such as PLA and PHBV (Huda et al. 2008; Singh et al. 2008; Suryanegara et al. 2009; Nyambo et al. 2010), natural rubber (Bras et al. 2010), and various biopolymers such as starch, alginate, and chitosan (Chen et al. 2009; Huq et al. 2012; Mesquita et al. 2012; Khan et al. 2012). As one of such biopolymers, agar has been considered as a good candidate for the preparation of bionanocomposite since it is abundantly available and renewable biopolymer with excellent film forming property, biodegradability, and biocompatibility (Rhim et al. 2011).

Therefore, the main objectives of the present study were to isolate cellulose nanocrystals from onion skin and prepare nanocomposite film by blending the cellulose nanofiber with agar for the value-added utilization of onion skin. To achieve the objectives, cellulose nanocrystals were obtained by acid hydrolysis and the effect of different concentration of H_2SO_4 (45, 55, and 65 %) was evaluated by Fourier transform infrared spectroscopy (FTIR), transmission electron microscopy (TEM), and thermogravimetric analysis (TGA). In addition, the effects of cellulose nanocrystals on the mechanical and water vapor barrier properties of the agar/CNC composites films were tested.

Experimental

Materials

Food grade agar was obtained from Fine Agar Co., Ltd. (Damyang, Jeonnam, Korea). Glycerol, sodium chlorite, sodium bisulfate, and ethanol were procured from Sigma Aldrich Co. (St Louis, MO, USA). Onion skins, produced as a by-product during the processing of onion, were obtained from a local food processing company.

Chemical composition

Onion skin was washed thoroughly with water to remove dirt and dried in an air oven at 105 °C for 24 h. The dried samples were ground into powder to get onion skin powder (OSP) and used for further analysis. The contents of α-Cellulose, hemicelluloses and lignin of the onion skin were determined according to the methods of quantitative analysis for grass fibers (Maheswari et al. 2012). The content of α-Cellulose, hemicellulose and lignin were determined using five replicated samples and the average values with standard deviation were reported.

Separation of cellulose microfibers

The onion skin sample was first bleached with 0.7 % (w/v) sodium chlorite solution (fiber to liquor ratio of 1:50) at pH 4, adjusted by 5 % acetic acid and maintained the same pH. The mixture was boiled for 2 h with stirring to remove lignin. The residue was subsequently washed with distilled water. The neutral residue was then boiled with 250 mL of 5 % (w/v) sodium sulfite solution for 5 h, followed by washing with distilled water to complete removal of lignin. The resulting component is a holocellulose composed of hemi-cellulose and α-Cellulose. The holocellulose was treated with 17.5 % sodium hydroxide solution at 20 °C for 45 min. The solution were filtered and treated with 10 % acetic acid to remove sodium hydroxide and washed with distilled water. Finally, extracted cellulose was dried at 105 °C to get cellulose microfiber (CMF).

Isolation of cellulose nanocrystals

Onion skin cellulose nanocrystals were isolated by acid hydrolysis using three different concentration of sulfuric acid (45, 55, and 65 % H_2SO_4). Briefly, 5 g of CMF was hydrolyzed by refluxing with sulfuric acid (fiber to liquor ratio of 1:20) at 60 °C for 3 h with strong agitation. The hydrolysis was quenched by adding excess amount of distilled water to the reaction mixture. The resulting mixture was cooled to room temperature. Thereafter, the suspension was repeatedly centrifuged at 4,000 rpm for 20 min using a centrifuge (Hanil Scientific Centrifuge, Incheon, Korea) and the supernatant was discarded until it became cloudy. The pH of the suspension was above 5. The suspension was sonicated using a high intensity ultrasonic processor (Model VCX 750, Sonics & Materials Inc., Newtown, CT, USA) for 5 min in an ice bath to avoid overheating. The cloudy suspension was then subjected to dialysis against distilled water until the water pH reached neutrality. Then, the suspension was freeze-dried to obtain cellulose nanocrystals (CNC). For this, the suspension was first frozen at deep freezer at −70 °C and transferred to a freeze dryer (PVTFD-10R, Ilshin Lab Co. Ltd., Yangju, Korea) and dried for about 72 h. The pressure in the drying chamber was set at 0.3 torr and the temperature in the condensing chamber was controlled at −40 °C. Sublimation heat was provided by a heater mat at 30 °C underneath the drying tray. The CNCs obtained were coded as CNC45, CNC55, and CNC65 according to the concentration of sulfuric acid used for the acid hydrolysis.

Preparation of agar-based composites films

Agar and agar-based nanocomoposite films were prepared using a solution casting method described by Rhim et al. (2011). Agar film was prepared by dissolving 4 g of agar powder in 150 mL of distilled water with 1.2 g of glycerol as plasticizer while mixing vigorously for 30 min at 95 °C using a magnetic stirrer and cast evenly onto a leveled Teflon film (Cole-Parmer Instrument Co., Chicago, IL, USA) coated glass plate (24 × 30 cm), then dried for about 24 h at room temperature (22 ± 3 °C). In addition, agar/OSP, agar/CMF, and agar/CNC nanocomposite films were prepared. For this, 0.2 g of OSP, CMF, or three different types of CNC powder were dispersed in 150 mL of distilled water and stirred for 1 h using a magnetic stirrer. The fully wetted suspensions were homogenized using a high shear mixer (T25 basic, Ika Labotechnik, Janke & Kunkel Gmbh & Co., KG Staufen, Germany) at 12,000 rpm for 10 min. Then, 4 g agar and 1.2 g glycerol were dissolved into the fiber suspension while mixing vigorously for about 30 min at 95 °C using a hot plate and then cast evenly onto a leveled Teflon film coated glass plate and followed the same procedures as described above. The dried films were peeled off from the casting plate and conditioned in a constant temperature humidity chamber set at 25 °C and 50 % relative humidity (RH) for at least 48 h before further test. The thickness of film samples was measured using a hand-held micrometer (Dial Thickness gauge 7301, Mitutoyo, Japan) at an accuracy of 0.01-mm.

Scanning electron microscopy (SEM)

For the SEM observation, OSP, CMF and fractured film samples were coated with Os using a vacuum sputter coater and the microstructure of fibers and CMFs were observed using a FE-SEM (S-4800, Hitachi Co., Ltd., Matsuda, Japan) operated at accelerating voltage (V_{acc}) of 10 kV and current (I_e) of 10 μA. Fractured film samples were obtained by immersing them in liquid nitrogen and fractured.

Transmission electron microscopy (TEM)

For the TEM observation, the CNC was dispersed in distilled water (0.01 wt%) and about 8 μL of the CNC solution was deposited onto a glow-discharged carbon-coated TEM grid (Farmvar film on 200 square mesh copper grid, Ted Pella Inc., Redding, CA, USA). After 10 min, the excess liquid was removed by blotting with a filter paper, allowed to dry and observed the microstructure of CNC using a transmission electron microscopy (TEM, JEM-2100F, JEOL Ltd., Tokyo, Japan). The length and diameter of CNC was determined using the internal scale.

FT-IR analysis

FT-IR spectra of OSP, CMF, and CNC samples were obtained using an Attenuated total reflectance-Fourier transform infrared (ATR-FTIR) spectrophotometer (TENSOR 37 spectrophotometer with OPUS 6.0 software, Billerica, MA, USA) in the range of 4,000–500 cm^{-1}.

XRD analysis

X-ray diffraction patterns of cellulose fiber samples were tested using a XRD diffractometer (PANalytical Xpert Pro XRD diffractometer, Amsterdam, Netherlands), operated at 40 kV and 30 mA, equipped with Cu Kα radiation at a wavelength of 0.154056 nm and a curved graphite crystal monochromator. The samples were prepared in the powder form for the analysis. Samples were scanned over the range of diffraction angle of $2\theta = 5°–50°$ with a scanning rate of 0.4°/min at room temperature.

The crystallinity index (CI) was calculated by the following equation (Gumuskaya et al. 2003):

$$CI = \frac{I_{200} - I_{am}}{I_{200}} \quad (1)$$

where I_{200} is the intensity of the 200 peak (at $2\theta = 22°$) and I_{am} is the intensity corresponds to the amorphous structure which showed the lowest intensity value between 22 and 16°, which was located at around $2\theta = 18°$.

The crystallite size (D) of the CNC was calculated by the Scherrer equation (Nazir et al. 2013).

$$D = \frac{K\lambda}{\beta_{1/2}\,Cos\theta} \quad (2)$$

where, K is a constant (0.94), λ is the X-ray wavelength (λ = 0.154056 nm), $\beta_{1/2}$ is the full width at the half maximum (FWHM) of the peak, and 2θ is Bragg's angle (22°).

Thermo-gravimetric analysis (TGA)

The thermal stability of the fiber samples was determined by using a thermogravimetric analyzer (Hi-Res TGA 2950, TA Instrument, New Castle, DE, USA). About 5 mg of samples were taken in standard aluminum cup and heated from room temperature to 600 °C at heating rate of 10 °C/min under a nitrogen flow of 50 cm^3/min. Empty cup was used as a reference.

Tensile properties

The tensile properties such as tensile strength (TS), elongation at break (%E), and elastic modulus (EM) of the biocomposite films were measured using an Instron universal testing machine (5565, Instron Engineering Corporation, Canton, MA, USA) following the standard test method ASTM D 882-88. For this, rectangular specimens (2.54 × 15 cm) of film samples were stretched at a cross-head speed of 50 mm/min from the initial gap separation of 50 mm. Ten replicates were tested for each sample and the average values were presented.

Water vapor permeability (WVP)

The WVP of agar and biocomposite films was determined using a modified ASTM method E96-95. First, water vapor transmission rate (WVTR) was determined gravimetrically. For this, a square film

sample (7.5 × 7.5 cm^2) was mounted horizontally on the top of WVP cup (2.5 cm in depth and 6.8 cm of diameter) made of poly (methyl methacrylate) containing 18 mL of distilled water. The film sample was layered on the cup with O-ring made of rubber, then covered with the cup lid and tightened using screws to prevent leakage of water vapor. The cup was placed in an environmental chamber set at 25 °C and 50 % RH with air current movement of 198 m/min. The cup was weighed every 1 h interval for the period of 8 h. The WVTR was determined from the slope of the steady-state (linear) portion of weight loss versus time curve. Then the WVP of the film was calculated using the following equation:

$$\mathrm{WVP} = \frac{\mathrm{WVTR} \times \mathrm{L}}{\Delta p} \quad (3)$$

where WVTR was the measured water vapor transmission rate (g/m^2 s), L was the mean film thickness (m), and Δp was the partial water vapor pressure difference (Pa) across both sides of the film.

Statistical analysis

Measurements of each property were triplicated for tensile and water vapor permeability with individually prepared films as the triplicate experimental units. The software package SPSS version 12.0 (SPSS Inc., Chicago, IL, USA) was used for the statistical analysis. One-way analysis of variance (ANOVA) was performed and the significant differences among the values of film samples were determined using Duncan's multiple range test with significant level of $p = 0.05$.

Results and discussion

Chemical composition

The chemical composition of onion skin was presented in Table 1. The major component of onion skin was α-Cellulose (41.1 %), followed by lignin (38.9 %), hemicelluloses (16.2 %), and extractives (3.8 %). The α-Cellulose content of onion skin was comparable to those of agricultural residues used for cellulose source such as core fiber kenaf (37–49 %), jute (41–48 %), and was higher than those of rice straw (32.0 %) or rice husk (28.6 %) (Li et al. 2007; Janewit et al. 2008). This result suggests that the onion skin has a high potential for obtaining natural cellulose for the production of green composite materials.

Table 1 Chemical composition of onion skin

	Composition (%)
α-Cellulose	41.1 ± 1.1
Lignin	38.9 ± 1.3
Hemicellulose	16.2 ± 0.6
Extractives	3.8 ± 0.0

Morphology of fibers

Cellulose microfiber (CMF) and cellulose nanocrystals (CNCs) were isolated from onion skin. Figure 1 shows appearance of onion skin, onion skin powder (OSP), CMF, and suspension of three different types of CNCs (CNC45, CNC55, and CNC65). Apparently, onion skin and its powder showed brown color, which is mainly due to the natural colorant like quercetin in the onion skin (Benítez et al. 2011). However, the brown color was disappeared in the CMF during the process of bleaching with sodium chlorite and extraction of cellulose fiber with sodium hydroxide solutions. Apparently, all the CNCs seemed to be well dispersed in water to form homogeneously dispersed suspension.

The morphology of OSP, CMF, and CNCs was observed using SEM and TEM, respectively (Fig. 2). The cell wall structure of the OSP (Fig. 2a) appeared like a skeletal with smooth surface which consisted of lignin, hemicelluloses, and other extractives. However, the surface of CMF was rough due to removal of the cementing materials as shown in Fig. 2b. Bleaching of onion skin fiber with $NaClO_2$ allowed removal of most of the lignin present in the onion fiber, which helped for further defibrillation. It has been reported that sodium chlorite at acidic pH induced rapid oxidation of lignin by the chlorine to make lignin soluble and to be removed (El-Sakhawy and Hassan 2007). In addition, the treatment of cellulose fiber with $NaClO_2$ and NaOH caused the disappearance of the skeletal structure resulting in the rough surface of the CMF (Bledzki et al. 2008). Figure 2 (c–e) also showed TEM images of CNC45, CNC55, and CNC65. As observed in TEM images, the shape of CNCs has not been influenced by the acid concentration used for the acid hydrolysis. The fibers, in general, exhibited fibrillar form though some agglomeration was

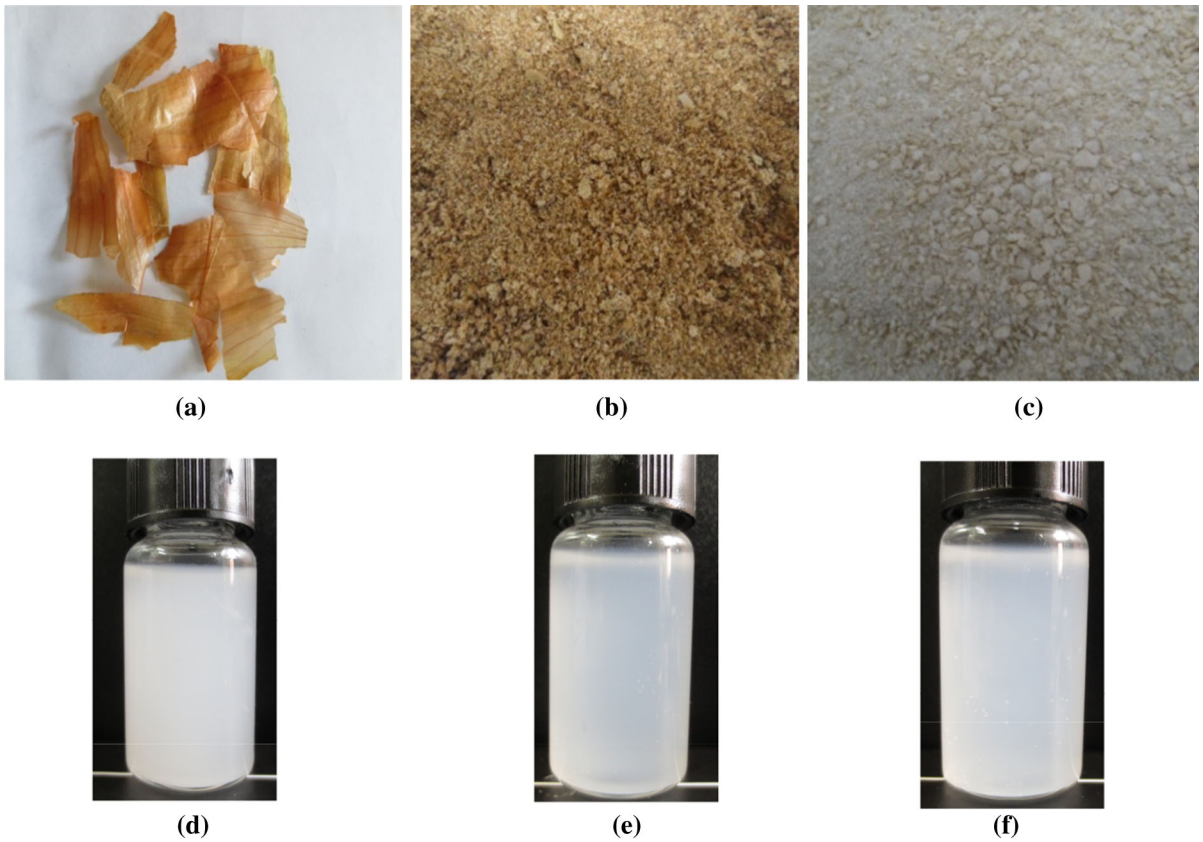

Fig. 1 Apparent shape of **a** onion skin, **b** onion skin powder (OSP), **c** onion skin cellulose microfiber (CMF), **d** CNC45, **e** CNC55, and **f** CNC65

observed depending on the acid concentration. Agglomeration of cellulose fibers were observed with CNC extracted with low concentration of acid (CNC45), however, CNC55 and CNC65 were in fibrillar structure with less agglomeration (Fig. 2d). It is interesting to note that the structure of CNCs became more fibrillar and non-agglomerated with increase in the acid concentration. It is probably because the amorphous region of microfibrils was cleaved transversely during sulfuric acid hydrolysis resulting in the reduction of fiber diameter from micrometer to nanometer (Azizi-Samir et al. 2005). Fiber size (length and diameter), aspect ratio, and yield of CNCs were presented in Table 2. The yield and fiber size of the CNCs were clearly dependent on the concentration of H_2SO_4 used for acid hydrolysis. The yield of CNCs decreased from 48.6 to 39.3 % with increase in acid concentration. The length and diameter of onion skin CNCs were in the range of 150–350 and 20–35 nm, respectively. The size of CNCs also decreased significantly ($p < 0.05$) with increase in acid concentration. Consequently, the aspect ratio of the CNCs decreased with increase in the acid concentration. Generally, the aspect ratio of CNCs is dependent on the source of fiber and CNC preparation methods. Han et al. (2014) also observed that the aspect ratio of cellulose nanoparticles isolated from microcrystalline cellulose decreased with increase in H_2SO_4 concentration. CNC with high aspect ratio is expected to give a good reinforcing effect, which may play an important role in improving the physical properties of composite materials.

FT-IR analysis

FT-IR spectra of OSP, CMF, and CNCs are shown in Fig. 3. The broad band observed at 3,353 cm^{-1}

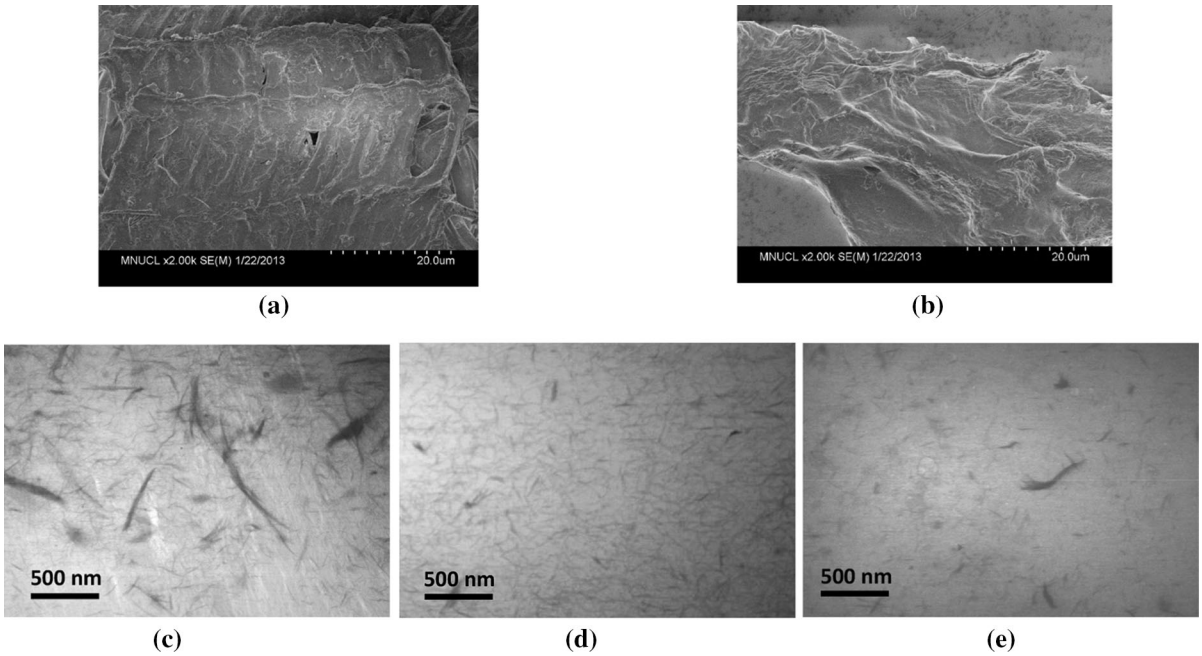

Fig. 2 Morphology of various types of onion skin cellulose fibers: SEM images of **a** OSP, **b** CMF, and TEM images of **c** CNC45, **d** CNC55, and **e** CNC65

Table 2 Dimension and yield of cellulose nanocrystals obtained from onion skin fibers

Nanocrystals	Length (nm)	Diameter (nm)	Aspect ratio	Yield (%)
CNC45	356 ± 85^{c}	35 ± 7^{c}	10.1	48.6
CNC55	220 ± 48^{b}	23 ± 3^{b}	9.5	43.2
CNC65	156 ± 18^{a}	20 ± 2^{a}	7.8	39.3

Each value is the mean of three replicates with the standard deviation. Any two means in the same column followed by the same letter are not significantly ($p > 0.05$) different by Duncan's multiple range tests

corresponds to O–H stretching of the cellulose and hemicellulose present in the fiber. The absorption peaks around 2,900 cm^{-1} for CMF and CNCs are due to the stretching vibration of C–H groups of cellulose. The intense peaks of OSP noted at 1,730 and 1,236 cm^{-1} correspond to the acetyl ester and carbonyl aldehyde group (C=O) stretching of hemicelluloses and lignin (Reddy et al. 2013). These peaks were disappeared in the spectra of CMF and CNCs, which were attributed to the removal of hemicellulose and lignin by $NaOCl_2$ and alkaline treatment. The intense peaks at 1,606 cm^{-1} observed in CMF and CNCs are

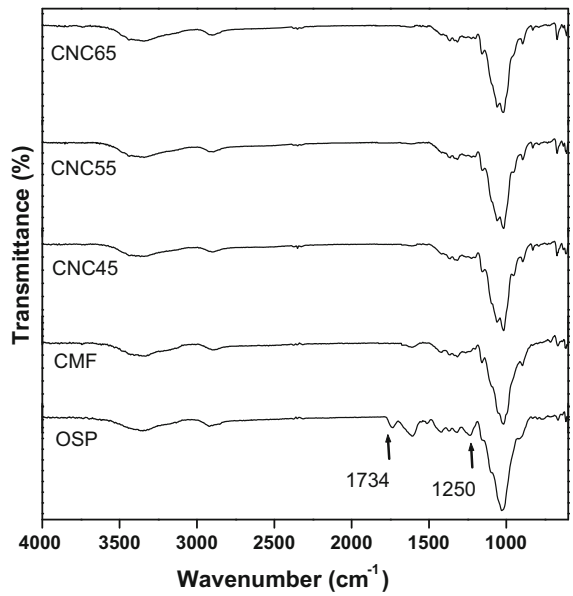

Fig. 3 FT-IR spectra of various types of onion skin cellulose fibers

related to absorbed moisture by the fibers. The bands at 1,426 and 1,325 cm^{-1} are corresponding to CH_2 scissoring and O–H bending vibration of cellulose,

respectively (Waleed and Maha 2003). Other two peaks at 1,061 and 897 cm^{-1} are associated with the C–O stretching and C–O–C deformation at the glycosidic linkage of cellulose which appeared in all of the spectra (Wada et al. 2004). The FT-IR spectra of CNCs are similar to that of CMF in all wave numbers, which indicates that the main cellulose structure was maintained during acid hydrolysis. However, in the case, the peak intensity of CNC was higher than that of CMF, which indicates that the crystallinity of the CNC increased. The most notable change in the CNCs was the appearance of two peaks at 1,032 and 1,017 cm^{-1}, whereas, only one peak was observed in CMF, which corresponds to C–O–C structure of β-(1, 4)-D-glucosidic linkage of cellulose. This may be caused by the breakage of glucosidic bond after acid hydrolysis. Moreover, there were no significant difference in FT-IR spectra and peak intensities among the CNCs, which indicates that the acid concentration did not affect the chemical structure of the CNCs.

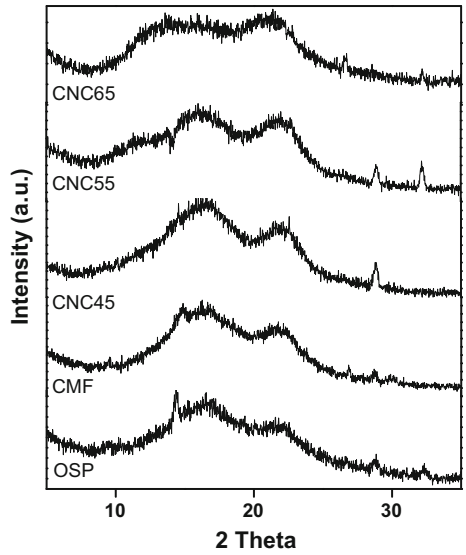

Fig. 4 XRD patterns of various types of onion skin cellulose fibers

XRD pattern

The effect of alkaline extraction and acid hydrolysis on the crystallinity of onion skin cellulose fibers was tested by XRD analysis. XRD patterns of the native fiber of OSP, CMF, and CNCs are shown in Fig. 4. All of the onion fibers, OSP, CMF, and CNCs revealed intense peaks at 2θ of 16.4° and 22.2°. A sharp intensive peak at 22.2° was observed for the natural fibers, which is a typical XRD pattern of the crystalline structure of the cellulose type I (Wada et al. 2004). However, this sharp peak has not been observed in both CMF and CNC samples, which is mainly due to the partial destruction of the Cellulose-I structure by the NaOH (17.5 %) treatment. The different differaction peaks in CMF and CNC might be due to that cellulose I in CMF has been converted to cellulose II after alkali treatment. Similar XRD pattern has been observed with the cellulose extracted from bean hull (Adel et al. 2010). The XRD patterns also exhibited that the intensities of the CMF and the CNCs were higher than that of native onion fiber and they also exhibited sharper peaks at 22° than the native onion fiber. These results indicate that the crystallinity of CMF and CNCs increased compared with the native onion fiber. The CI and crystallite size of the fibers are presented in Table 3. The CI of native fiber and CMF were 0.21 and 0.24, respectively. The increase in crystallinity of the CMF was mainly due to the removal of amorphous hemicellulose and lignin as evidenced by the chemical analysis (Rajulu et al. 2002). The result was also supported by the results of FT-IR analysis. The CI was further increased after isolation of CNCs, but the CI of CNCs were affected by the acid concentration used for hydrolysis. The CI of CNC45 was 0.26 and increased up to 0.30 with acid concentration of 55 %, and then decreased down to 0.27 with acid concentration of 65 %. The increase in crystallinity of CNCs was due to the hydrolysis of glucosidic linkages in the accessible regions of cellulose fibers, which was accompanied by a significant increase in the crystalline fraction with the loss of a disordered soluble fraction of the polymer (Adel et al. 2010). However, the CI of CNC65 decreased compared to the other types of CNC. This result can be

Table 3 Crytallinity index (CI) and crystallite size of onion skin fibers

Fiber type	CI	Crystallite size (nm)
OSP	0.21	2.01
CMF	0.24	2.11
CNC45	0.26	2.73
CNC55	0.30	2.49
CNC65	0.27	1.76

explained by the XRD patterns. The XRD peaks of CNCs at 22.5° increased with an increase in acid concentration up to 55 %, and there was no obvious increase in the relative intensity of this diffraction peak with further increase in the acid concentration. This was presumably due to the dissolution of cellulose to form regenerated cellulose with polymorph with high acid concentration, resulting in the reduction in crystallinity of cellulose (Ioelovich 2012b). Pan et al. (2013) tested the effect of acid concentration (20, 40, and 60 wt% H_2SO_4) on the crystallinity of cellulose nanowhiskers (CNWs) isolated from a commercial microcrystalline cellulose (MCC), and they also found that the CI of CNWs increased with increase in acid concentration. Table 3 also shows the crystallite size of the OSP, CMF, and CNCs. On the contrary to the CI, crystallite size of onion skin cellulose decreased continuosly with the processing of alkaline extraction and acid hydrolysis of cellulose fiber. In addition, the crystallite size of CNCs decreased monotonically with increase in acid concentration for the hydrolysis. It is probable that the higher concentration of acid with stronger hydrolysis power would remove amorphous domains more effectively and break the bundle of cellulose fiber to form a less crystallite of CNC (Das et al. 2009).

Thermal stability

Thermal stability of the OSP, CMF, and CNCs was tested using TGA and the resulting TGA thermograms and DTG curves were shown in Fig. 5. The TGA of various types of onion fibers revealed three main weight loss regions. The first region at temperature of 80–200 °C was due to the evaporation of physically weak and chemically strong bound water, and the weight loss of the film in those ranges is about 8 wt°%. In this region, the weight change of CNCs was seemingly higher than that of OSP and CMF. It is because the moisture content of CNCs is lower than the OSP or CMF due to the dehydration of cellulose fibers occurred during the acid hydrolysis. Sulfate groups introduced at the outer surfaces of CNCs during acid hydrolysis of cellulose fiber are known to induce dehydration of the fiber (Roman and Winter 2004; Wang et al. 2007). The second transition of thermal degradation was observed at around 200–330 °C with the total weight loss of about 21, 18, and 28 % for OSP, CMF, and CNCs, respectively.

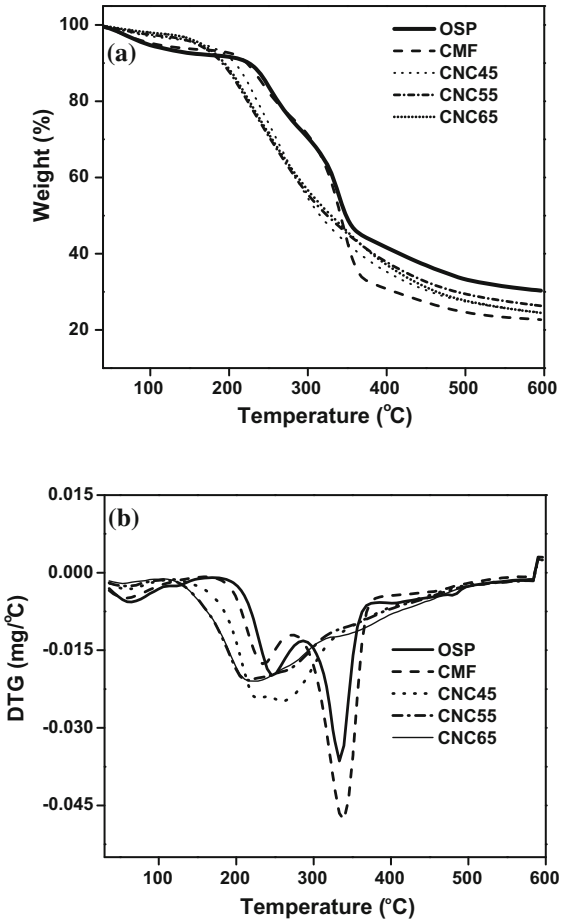

Fig. 5 TGA thermograms and DTG curves of various types of onion skin cellulose fibers

The thermal degradation temperature of CNCs at this stage was lower than that of OSP and CMF. The thermal degradation of CMF was less than that of OSP since most of hemicellulose and lignin were removed from the cellulose fibers (Reddy et al. 2009). The third stage of weight loss occurred around 330–370 °C depending on the type of cellulose fibers, which is mainly due to the cleavage of cellulose backbone or the decomposition of carbonaceous matter. At this stage, the thermal degradation temperature of the CNCs was significantly lower than those of OSP and CMF. The thermal degradation temperature of CNCs decreased with increase in acid concentration. The decrease in thermal stability of the CNC may be due to the introduction of sulfated groups into nanocrystals during the sulfuric acid hydrolysis of the fiber (Roman and Winter 2004). The sulfate groups introduced to the

outer surfaces of cellulose caused dehydration of cellulose fiber and this probably cused the reduced thermal stability of the CNC (Roman and Winter 2004; Reddy and Rhim 2014).

The final residue (i.e., char remained at 600° C) of the OSP, CMF and CNCs were 30, 22, and 24 %, respectively. Higher amount of residual content of the OSP was mainly due to the lignin and hemicellulose content (Maheswari et al. 2012). However, the amount of residue for CNC45, CNC55, and CNC65 was higher than CMF. Similar behavior of thermal degradation has been observed for the nanocellulose extracted from rice straw and cotton fibers and explained that the dehydration of CNCs by the sulfate groups was responsible for higher amount of residue of nanocrystals (Jiang and Hsieh 2013; Lu and Hsieh 2010).

Microstructure of biocomposite films

The morphology of cross-section of the composite films were observed using SEM as shown in Fig. 6. Loosely formed composite film was formed between agar and OPS powder, in which OPS was not well distributed in the polymer matrix. This is mainly because that the natural fiber contains many extractives such as waxes, pectin and other materials which restricts the interfacial adhesion with the polymer matrix. On the contrary, smooth-surfaced flexible composite films were formed with both CMF and CNC (Fig. 6 b, c) indicating that the affinity between fibers and agar has been increased after removal of undissolvable extractives from the OSP. It is generally known that the chemical treatment of natural fibers leads to defibrillation of the fiber, which could improve the roughness of the surface and hence enhance the adhesion between the fiber and polymer matrix to form more uniform composite films.

Mechanical properties of biocomposite films

Tensile properties such as tensile strength (TS), elongation at break (E), and Young's modulus (YM) of agar, agar/OSP, agar/CMF, and agar/CNCs composite films were tested using an Instron universal testing machine and the results are shown in Table 4. The TS of all the composite films except agar/CNC45 composite film decreased significantly ($p < 0.05$) compared with pristine agar film. In the case of agar/OSP and agar/CMF composite films, the TS decreased about 43 and 37 %, respectively, compared with that of pristine agar film. The reduction in TS is partly due to the random orientation of the native fibers in the agar polymer matix, and mainly due to the poor interfacial adhesion between the fiber and matrix, especially for agar/OSP and agar/CMF films (Li et al. 2010). However, the TS of agar/CNCs composite films increased appreciably compared to those of agar/OSP and agar/CMF films. This could be due to the formation of the rough surface of nanocrystals during the hydrolysis of fiber with sulfuric acid, which induced the formation of hydrogen bond between the agar and the nanocrystals (Agustin et al. 2013). In addition, the chemical treatment of natural fibers leads to the defibrillation on the surface of the fiber, which improve the roughness of the surface hence the fiber matrix adhesion increased to form a stronger composite film.

Among the agar/CNCs composite films, agar/CNC45 had the highest TS, and the TS of the agar/CNC composite film decreased with increase in the acid concentration for hydrolysis of fiber. The difference in TS between agar/CNC composite films may be attributed to the difference in the aspect ratio of the CNCs as shown in Table 2. Chen et al. (2009) also found that the mechanical properties of pea starch and cellulose nanowhiskers hydrolyzed from pea hull fiber were greatly influenced by the variation of aspect ratio of cellulose nanowhiskers induced by the different hydrolysis time. On the contrary, there was no appreciable changes in the flexibility of the composite films determined by the elongation at break (E). The stiffness of the films determined by the YM exhibited a similar trend as the TS of the composite films. The tensile test results of agar/CNCs composite films indicated that CNC45 exhibited the highest mechanical strength of agar/CNC composite film. Therefore, CNC45 was chosen to test the effect of filler concentration on the mechanical and water vapor barrier properties of agar/CNC composite film. Figure 7 shows the effect of CNC45 concentration on tensile properties of the agar/CNC45 composite films. The TS of agar film increased linearly from 50.6 ± 4.3 up to 57.2 ± 2.1 MPa with loading of the nanofiller from none to 3 wt%, and then decreased. The YM of the composite film showed the similar pattern as the TS (data not shown). This improvement in tensile strength and modulus of the bio-nanocomposites could be associated with very high stiffness of CNC (YM in the

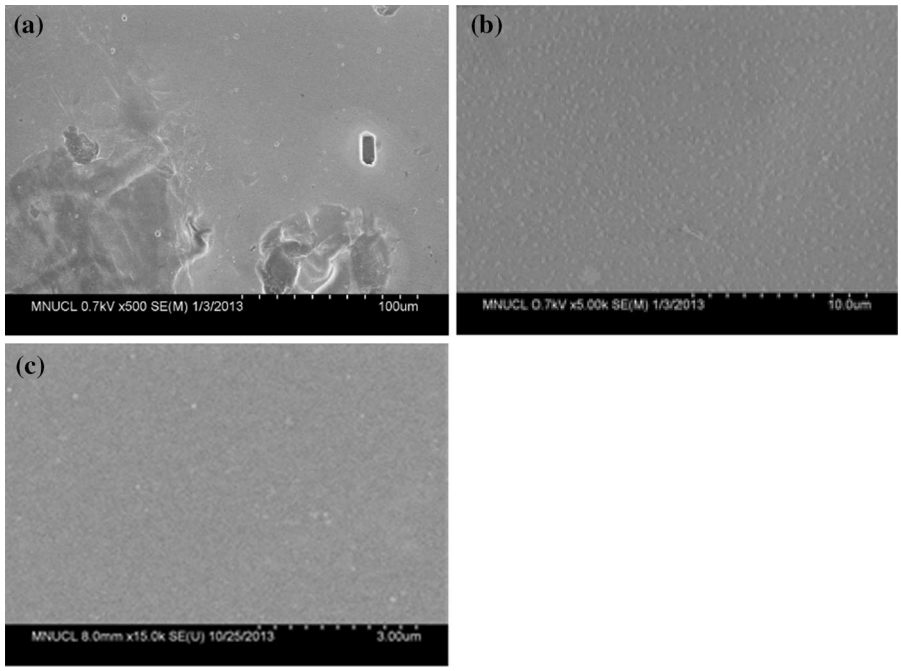

Fig. 6 SEM images of fractured surface of composite film **a** Agar/OSP, **b** Agar/CMF, **c** Agar/CNC45

Table 4 Tensile properties and water vapor permeability (WVP) of agar and agar/onion skin fiber composite films

Film	Thickness (μm)	TS (MPa)	E (%)	YM (GPa)	WVP ($\times 10^{-9}$ g m/m^2 s Pa)
Agar	55.7 ± 1.0^{a}	50.6 ± 4.3^{d}	25.4 ± 4.4^{c}	1.64 ± 0.08^{b}	2.02 ± 0.06^{a}
Agar/OSP	92.4 ± 1.6^{e}	28.8 ± 1.6^{a}	19.2 ± 5.4^{a}	1.16 ± 0.10^{a}	3.27 ± 0.73^{c}
Agar/CMF	83.7 ± 1.9^{d}	32.1 ± 2.5^{a}	24.0 ± 2.6^{bc}	1.10 ± 0.09^{a}	2.60 ± 0.19^{b}
Agar/CNC45	60.7 ± 1.0^{c}	50.0 ± 4.7^{d}	21.9 ± 4.9^{ab}	1.98 ± 0.20^{c}	1.78 ± 0.04^{a}
Agar/CNC55	59.3 ± 2.0^{bc}	43.8 ± 5.2^{c}	21.7 ± 3.1^{ab}	1.63 ± 0.16^{b}	1.89 ± 0.14^{a}
Agar/CNC65	57.7 ± 2.1^{b}	40.3 ± 1.8^{b}	25.6 ± 4.3^{c}	1.45 ± 0.18^{b}	1.84 ± 0.15^{a}

Each value is the mean of three replicates with the standard deviation. Any two means in the same column followed by the same letter are not significantly ($p > 0.05$) different by Duncan's multiple range tests

Fiber content was 5 wt% based on agar

range of 130–250 GPa) with the high aspect ratio. However, the TS of the composite film decreased compared with that of agar/CNC3 % composite films when higher content of CNC (5 wt%) was incorporated. This may be attributed to the agglomeration of the fiber at higher content of CNC. The elongation at break (E) of the films increased slightly by blending with the nanofiller up to 3 wt%, and then decreased at higher concentration of the nanofiller (5 wt%). Usually, the E of films is known to be varied inversely with the TS. Though the E of agar/CNC45 films showed similar changes like the TS, however, the change was not so significant. It has been reported that fibrous network formed between cellulosic nanofiber and polymer matrices keeps the elasticity of the composite films (Missoum et al. 2013). Mandal and Chakrabarty (2014) also observed the similar behavior in the cellulose nanocrystal-reinforced PVA composites. They reported that the increase in the E at low content of cellulose nanofiller was due to the formation of hydrogen bonds between them, and the interaction has been disturbed at high content of nanofiller resulting in the decrease in the E.

Water vapor permeability (WVP)

Table 4 also shows the results of WVP of agar, agar/OSP, agar/CMF, and agar/CNCs composite films. The

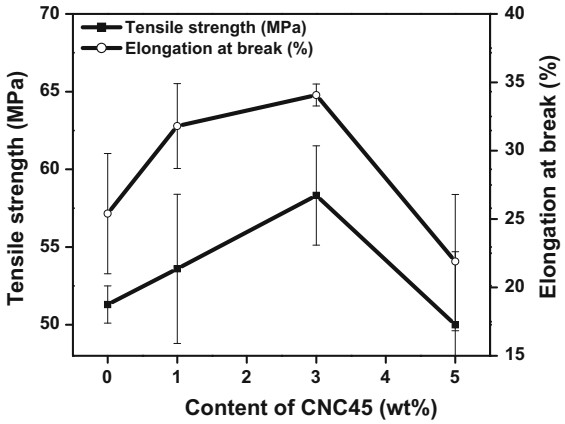

Fig. 7 Effect of nanofiller content on the tensile properties of the agar/CNC45 composite films

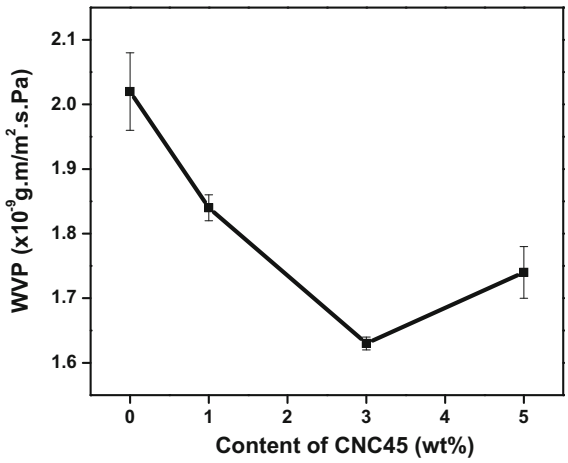

Fig. 8 Effect of nanofiller content on the WVP of the agar/CNC45 composite films

WVP of the pristine agar film was 2.02×10^{-9} g m/m^2 s Pa. It was affected by the type of onion skin cellulose fibers. The WVP of the composite film blended with OSP was significantly higher than that of the pristine agar film. This might be due to the poor interfacial attraction between the OSP and the biopolymer matrix, which probably increased the diffusion rate of water vapor through the void between the fiber and agar. The untreated OSP fiber has a smooth surface with extractives, which probably made a void between the agar and the OSP fiber and thus increased the water vapor permeation rate. The WVP of agar/CMF composite film was significantly lower than that of agar/OSP film, but it was still significantly higher than that of the agar film. The decreased WVP of agar/CMF composite film compared with the agar/OSP composite film might be due to the less interfacial gap between the fiber and agar caused by the removal of wax, hemicellulose, and lignin during cellulose extraction from the OSP. However, the WVP of agar films decreased down to the level of 1.78–1.89 $\times$ 10^{-9} g m/m^2 s Pa after formation of composite with CNCs. The WVP of agar/CNCs composite films were significantly ($p < 0.05$) lower than those of agar/OSP and agar/CMF composite films, and they were even lower than that of agar pristine film though the difference was not statistically significant. The decrease in WVP of agar/CNC composite films is believed to be due to the presence of crystalline nanoparticles dispersed in the agar polymer matrix. The impermeable nanoparticles with high aspect ratio forces the water vapor travel through the film to follow a tortuous path through the polymer matrix surrounding the particles, thereby increases the effective path length for diffusion (Rhim et al. 2011). Though the difference was not significant, agar/CNC45 showed the lowest WVP among the agar/CNCs composite films tested. Therefore, to test the effect of CNC content on the WVP, CNC composite film with different content of nanofiller was tested with CNC45 and the results were shown in Fig. 8. As shown in Fig. 8, the WVP of agar/CNC45 composite films was strongly dependent on the content of nanofiller. The WVP of agar/CNC45 composite film decreased linearly with increase in the nanofiller content up to 3 wt% of CNC45 and then increased with further increase in the nanofiller content. At the higher content of CNC45 (5 wt%), the CNC may not be uniformly dispersed through the polymer matrix due to the agglomeration of the CNC, which probably caused the increased water vapor permeability of the composite film.

Based on the results of tensile test and water vapor permeability measurement, it can be concluded that 3 wt% of CNC45 loading into agar film is the optimum for the improvement of mechanical and water vapor barrier properties of agar-based film.

Conclusions

The cellulose microfiber was extracted from onion skin cellulose fiber by alkaline extraction and the

nanocrystals were isolated from the extracted cellulose microfiber by acid hydrolysis using H_2SO_4 solution. The effect of acid concentration on the characteristics of cellulose nanocrystals was tested using SEM, XRD, FT-IR, and TGA, and reinforcing effect as a nanofiller of the different types of cellulose nanocrystals was evaluated through preparation of agar/cellulose nanocrystals nanocomposite films. Not only the yield but also the properties of onion skin cellulose nanocrystals such as CI, crystallite size, and thermal stability were greatly influenced by the acid concentration used for hydrolysis of microcrystalline cellulose. Film properties evaluated with tensile strength, Young's modulus, and water vapor permeability indicated that the nanocrystals isolated with lower concentration (45 %) of H_2SO_4 was better compared with higher concentration of acid. These results suggested that the acid hydrolysis with 45 % of H_2SO_4 at 60° C for 3 h was the optimum condition for the extraction of CNC from onion skin cellulose fiber. The film properties of agar/CNC45 composite films were also dependent on the content of the nanofiller. With the loading of 3 wt% of nanocrystals (CNC45), the composite film had the highest tensile strength with the lowest water vapor permeability. This results indicates that different types of cellulose nanocrystals can be isolated from agricultural cellulosic resources such as onion skin and the resulting cellulose nanocrystals can be successfully utilized as a filler for the preparation of bionanocomposite films whose properties can be fine-tuned depending on the applications.

Acknowledgments This research was supported by iPET (Korea Institute of Planning and Evaluation for Technology in Food, Agriculture, Forestry and Fisheries), Ministry for Food, Agriculture, Forestry and Fisheries, Republic of Korea.

References

Adel AM, El–Wahab ZHA, Ibrahim AA, Mona TAS (2010) Characterization of microcrystalline cellulose prepared from lignocellulosic materials. Part I. Acid catalyzed hydrolysis. Bioresour Technol 101:4446–4455

Agustin MB, Ahmmad B, Richel EPDL, Jerico LB, Joel RS, Fumihiko H (2013) Starch-based biocomposite films reinforced with cellulose nanocrystals from garlic stalks. Polym Compos 34:1325–1332

Akaranta O, Efanga DE (1997) Dyeability of textile fibers with azo compounds prepared by coupling red onion skin extract with diazonium salts. J Nat Sci SriLanka 25:121–126

Alemdar A, Sain M (2008) Isolation and characterization of nanofibers from agricultural residues wheat straw and soy hulls. Bioresour Technol 99:1664–1671

Azizi-Samir MAS, Alloin F, Dufresne A (2005) Review of recent research into cellulosic whiskers, their properties and their application in nanocomposite field. Biomacromolecules 6:612–626

Beck-Candanedo S, Roman M, Gray DG (2005) Effect of reaction conditions on the properties and behavior of wood cellulose nanocrystal suspensions. Biomacromolecules 6:1048–1054

Benítez V, Mollá E, Martín-Cabrejas MA, Aguilera Y, López-Andréu FJ, Cools K, Terry LA, Esteban RM (2011) Characterization of industrial onion wastes (*Allium cepa* L.): dietary fiber and bioactive compounds. Plant Foods Hum Nutr 66:48–57

Bledzki AK, Mamun AA, Gabor ML, Gutowski VS (2008) The effects of acetylation on properties of flax fiber and its polypropylene composites. Express Polym Lett 2:413–422

Bondeson D, Mathew A, Oksman K (2006) Optimization of the isolation of nanocrystals from microcrystalline cellulose by acid hydrolysis. Cellulose 13:171–180

Bras J, Hassan ML, Bruzesse C, Hassan EA, El-Wakil NA, Dufresne A (2010) Mechanical, barrier, and biodegradability properties of bagasse cellulose whiskers reinforced natural rubber nanocomposites. Ind Crop Prod 32:627–633

Chen Y, Liu C, Chang PR, Cao X, Anderson DP (2009) Bionanocomposites based on pea starch and cellulose nanowhiskers hydrolyzed from pea hull fibre: effect of hydrolysis time. Carbohydr Polym 76:607–615

Das K, Ray D, Bandyopadhyay NR, Ghosh T, Mohanty AK, Misra M (2009) A study of the mechanical, thermal and morphological properties of microcrystalline cellulose particles prepared from cotton slivers using different acid concentrations. Cellulose 16:783–793

El-Sakhawy M, Hassan ML (2007) Physical and mechanical properties of microcrystalline cellulose prepared from agricultural residues. Carbohydr Polym 67:1–10

Gumuskaya E, Usta M, Kirci H (2003) The effects of various pulping conditions on crystalline structure of cellulose in cotton linters. Polym Degrad Stab 81:559–564

Han G, Huan S, Han J, Zhang Z, Wu Q (2014) Effect of acid hydrolysis conditions on the properties of cellulose nanoparticle-reinforced polymethylmethacrylate composites. Materials 7:16–29

Henriksson M, Henriksson G, Berglund LA, Lidström T (2007) An environmentally friendly method for enzyme-assisted preparation of microfibrillated cellulose (MFC) nanofibers. Eur Polym J 43:3434–3441

Herrick FW, Casebier RL, Hamilton JK, Sandberg KR (1983) Microfibrillated cellulose: morphology and accessibility. J Appl Polym Sci Appl Polym Symp 37:797–813

Hubbe MA, Rojas OJ, Lucia LA, Sain M (2008) Cellulose nanocomoposites: a review. Bioresources 3:929–980

Huda MS, Drzal LT, Mohanty AK, Misra M (2008) Effect of fiber surface-treatments on the properties of laminated biocomposites from poly(lactic acid) (PLA) and kenaf fibers. Comp Sci Technol 68:424–432

Huq T, Salmieri S, Khan A, Khan RA, Tien CL, Riedl B, Fraschin C, Bouchard J, Uribe-Calderon J, Kamal MR, Lacroix M (2012) Nanocrystalline cellulose (NCC)

reinforced alginate based biodegradable nanocomposite film. Carbohydr Polym 90:1757–1763
Ioelovich M (2012a) Study of cellulose interaction with concentrated solutions of sulfuric acid. ISRN Chem Eng 428974:1–7
Ioelovich M (2012b) Optimal conditions for isolation of nanocrystalline cellulose particles. Nanosci Nanotechnol 2:9–13
Janewit W, Nakorn W, Suneerat P (2008) Product yields and characteristics of rice husk, rice straw and corncob during fast pyrolysis in a drop-tube/fixed-bed reactor. Songklanakarin J Sci Technol 30:393–404
Jiang F, Hsieh YL (2013) Chemically and mechanically isolated nanocellulose and their self-assembled structures. Carbohydr Polym 95:32–40
Khan A, Khan RA, Salmieri S, Tien CL, Riedl B, Bouvhard J, Chauve G, Tan V, Kamal MR, Lacroix M (2012) Mechanical and barrier properties of nanocrystalline cellulose reinforced chitosan based nanocomposite films. Carbohydr Polym 90:1601–1608
Khan A, Huq T, Khan RA, Riedl B, Lacroix M (2014) Nanocellulose-based composites and bioactive agents for food packaging. Crit Rev Food Sci Nutr 54:163–174
Komolwanich T, Tatijarern P, Prasertwasu S, Khumsupan D, Chaisuwan T, Luengnaruemitchai A, Wongkasemjit S (2014) Comparative potentiality of kans grass (*Saccharum spontaneum*) and giant reed (*Arundo donax*) as lignocellulosic feedstocks for the release of monomeric sugars by microwave/chemical pretreatment. Cellulose. doi:10.1007/s10570-013-0161-7
Li X, Tabil LG, Panigrahi S (2007) Chemical treatments of natural fiber for use in natural fiber-reinforced composites: a review. J Polym Environ 15:25–33
Li Y, Zhang J, He J, Reddy JP, Rajulu AV (2010) Tensile properties of hildegardia fibers reinforced polypropylene biocomposites. J Compos Mater 44:1681–1687
Limayema A, Ricke SC (2012) Lignocellulosic biomass for bioethanol production: current perspectives, potential issues and future prospects. Prog Energy Combust Sci 38:449–467
Lu P, Hsieh YL (2010) Preparation and properties of cellulose nanocrystals: rods, spheres, and network. Carbohydr Polym 82:329–336
Ludueina L, Fasce D, Alvarez VA, Stefani PM (2011) Nanocellulose from rice husk following alkaline treatment to remove silica. BioResources 6:1440–1453
Maheswari CU, Reddy KO, Muzenda M, Guduri BR, Rajulu AV (2012) Extraction and characterization of cellulose microfibrils from agricultural residue-*Cocos nucifera* L. Biomass Bioenerg 46:555–563
Mandal A, Chakrabarty D (2014) Studies on the mechanical, thermal, morphological and barrier properties of nanocomposites based on poly(vinyl alcohol) and nanocellulose from sugarcane bagasse. J Ind Eng Chem 20:462–473
Mesquita JP, Donnici CL, Teixeira IF, Pereira FV (2012) Bio-based nanocomposites obtained through covalent linkage between chitosan and cellulose nanocrystals. Carbohydr Polym 90:210–217
Missoum K, Martoïa F, Belgacem MN, Bras J (2013) Effect of chemically modified nanofibrillated cellulose addition on the properties of fiber-based materials. Ind Crop Prod 48:98–105
Nazir MS, Wahjoedi BA, Yussof AW, Abdullah MA (2013) Eco-friendly extraction and characterization of cellulose from oil palm empty fruit bunches. Bioresources 8:2161–2172
Nyambo C, Mohanty AK, Misra M (2010) Polylactide-based renewable green composites from agricultural residues and their hybrids. Biomacromolecules 11:1654–1660
Oksman K, Etang JA, Mathew AP, Jonoobi M (2011) Cellulose nanowhiskers separated from a bio-residue from wood bioethanol production. Biomass Bioenergy 35:146–152
Padma SV, Rakhi S (2009) Dyeing of cotton, wool and silk with extract of *Allium cepa*. Pigment Resin Technol 38:242–247
Pan M, Zhou X, Chen M (2013) Cellulose nanowhiskers isolation and properties from acid hydrolysis combined with high pressure homozinization. Bioresources 8:933–943
Rajulu AV, Rao GB, Rao BRP, Reddy AMS, He J, Zhang J (2002) Properties of ligno-cellulose fiber Hildegardia. J Appl Polym Sci 84:2216–2221
Reddy JP, Rhim JW (2014) Isolation and characterization of cellulose nanocrystals from garlic skin. Mater Lett 129:20–30
Reddy KO, Maheswari CU, Reddy DJP, Rajulu AV (2009) Thermal properties of Napier grass fibers. Mater Lett 63:2390–2392
Reddy K, Maheswari UC, Mukul S, Song JI, Rajulu AV (2013) Tensile and structural characterization of alkali treated borassus fruit fine fibers. Compos B 44:433–438
Rhim JW, Lee SB, Hong SI (2011) Preparation and characterization of agar/clay nanocomposite films: the effect of clay type. J Food Sci 76:40–48
Roman M, Winter WT (2004) Effect of sulfate groups from sulfuric acid hydrolysis on the thermal degradation behavior of bacterial cellulose. Biomacromolecules 5:1671–1677
Santos RMD, Neto WPF, Silvério HA, Martins DF, Dantas NO, Pasquini D (2013) Cellulose nanocrystals from pineapple leaf, a new approach for the reuse of this agro-waste. Ind Crop Prod 50:707–714
Singh S, Mohanty AK, Sugio T, Takai Y, Hamada H (2008) Renewable resource based biocomposites from natural fiber and polyhydroxybutyrate-co-valerate (PHBV) bioplastic. Compos A 39:875–886
Siro I, Plackett D (2010) Microfibrillated cellulose and new nanocomposite materials: a review. Cellulose 17:459–494
Suryanegara L, Nakagaito AN, Yano H (2009) The effect of crystallization of PLA on the thermal and mechanical properties of microfibrillated cellulose-reinforced PLA composites. Comps Sci Technol 69:1187–1192
Wada M, Heux L, Sugiyama J (2004) Polymorphism of cellulose I family: reinvestigation of cellulose IV. Biomacromolecules 5:1385–1391
Waleed KEZ, Maha MI (2003) Synthesis and characterization of cellulose resins. Polym Adv Technol 14:623–631
Wang N, Ding E, Cheng R (2007) Thermal degradation behaviors of spherical cellulose nanocrystals with sulfate groups. Polymer 48:3486–3493
Yu L, Dean L, Li L (2006) Polymer blends and composites from renewable resources. Prog Polym Sci 31:576–602